Intermittent fireline behaviour over porous vegetative media in different crossflow conditions

Abhinandan Singh[A,*] [iD], Reza M. Ziazi[A] [iD] and Albert Simeoni[A]

For full list of author affiliations and declarations see end of paper

*Correspondence to:
Abhinandan Singh
Department of Fire Protection Engineering,
Worcester Polytechnic Institute,
Worcester, MA, USA.
Email: asingh4@wpi.edu

ABSTRACT

Background. Reliable wildfire prediction and efficient controlled burns require a comprehensive understanding of physical mechanisms controlling fire spread behaviour. Earlier studies explored the intermittent nature of free-burning fires, but the influence of flame intermittency on fire spread requires further attention. **Aims.** This research qualitatively explores dynamic fire behaviour and its influence on fire spread. **Methods.** Fire spread experiments were conducted under varying wind conditions inside a wind tunnel. Various cameras were used for qualitative analysis, verified against velocity and temperature measurements carried out inside the fuel bed. **Key results.** Dynamic fire behaviour was observed in the form of near-bed flame pulsations. These pulsations caused fluctuating contact between the flame and unburned fuel ahead of the fire front, leading to point ignitions. Under favourable heat transfer conditions, these point ignitions strengthened and merged with the existing fire front, leading to intermittent flame spread in the form of leaps. **Conclusions.** The transient nature of flame spread was observed during fire spread experiments conducted under steady external conditions. **Implications.** This research lays the foundation for critical flow and heat transfer analyses required to characterise intermittent flame spread.

Keywords: fire spread, flame leaping, flame pulsation, flame residence, ignition, intermittency, porous media, vegetative fire.

Introduction

Owing to a lack of technical literature and limited understanding of wood fires, forestry organisations in North America focused on fire exclusion, leading to unprecedented fuel accumulation in forests (Brown and Davis 1973). There is an increased importance on conducting efficient land management, not only owing to the presence of dense surface vegetation (Hann and Bunnell 2001) but also because of an increase in fuel dryness (Arnell et al. 2019) and expanding wildland–urban interface (WUI) (Radeloff et al. 2018). Indigenous people used fire for land management (Kimmerer and Lake 2001), preventing large wildfires and enhancing biodiversity (Trauernicht et al. 2015). Therefore, the focus has shifted toward controlled burns to counter the current wildfire problem.

Prescribed or controlled burns require significant planning to reduce the possibility of uncontrolled conflagrations, which can lead to losses (Romero 2022). The window for safe controlled burns has diminished owing to rising global temperatures, which makes fundamental fire research vital. Comprehensive review articles (Perry 1998; Sullivan 2009a, 2009b, 2009c; Liu et al. 2021) provide state-of-the-art fire spread research and are of importance in finding research gaps. A considerable portion of the fire literature focuses on average fire spread behaviour while giving little insight into dynamic fire behaviour and its influence on fire spread. Current research tries to close this gap by experimentally evaluating intermittent flame spread and its controlling parameters from a qualitative perspective.

Various stationary and spreading fires using burners (Tang et al. 2019), pool fires (Lin et al. 2021), cribs (McAllister and Finney 2016), engineered cardboards (Finney et al.

2015) and vegetative fuels (Simpson *et al.* 2014) have been used to explore pulsating fire behaviour. Stationary fires are commonly used for such analyses to increase the ease of experimental procedures and for better control over external conditions. The conclusions from such experimental studies might not work during practical fire spread situations and can lead to the development of prediction models with limited application. Therefore, experimental research emulating a natural environment works better to develop reliable fire prediction models.

A significant portion of wildfire research considers fire spread as a continuous movement of flame occurring with subsequent ignition of unburned fuel ahead of the fire front (Rothermel 1972; Albini 1985, 1986; Dupuy 1995; Catchpole *et al.* 1998; Pastor *et al.* 2006). However, the multi-scale interaction between wind, fire and topography (Simeoni 2013) makes fire spread a dynamic phenomenon that can influence the development of a fire and requires attention for building reliable prediction models. Recent work by Viegas *et al.* (2021) explored the non-continuous nature of fire spread through various experiments. This work explored the variation in flame geometry (flame angle) due to changing buoyant conditions and its role in the non-monotonic nature of fire spread. In comparison, the research presented in the present paper explores flame pulsations and their influence on fire spread, which are different from the mean geometrical characteristics.

Flame pulsations during fire spread were first explored in the trench effect (Smith 1992; Atkinson *et al.* 1995), where pressure pulsations were measured by placing probes along the flame spread direction. The physical controlling mechanism generating these pressure variations was observed to change with the trench orientation. The frequency and magnitude of these pulsations were inversely related (Atkinson *et al.* 1995). Recent work by Finney *et al.* (2015) examined flame intermittencies and described the importance of convective heating for fire propagation. Delayed ignition due to intermittent particle heating was also analysed, and continuous flame presence was shown to be necessary for particle ignition and hence fire spread.

The current work builds on the understanding gained from Finney *et al.* (2015) and investigates the effect of flame contact on fire spread. The fuel particle ignition study presented in Finney *et al.* (2015) was for laser-cut cardboard combs. A significant contribution of the current work is the use of pine needles and observing their ignition relative to flame pulsation. It is reported by Finney *et al.* (2015) that flame contact is imperative for fire to spread. In comparison, the present study shows that flame contact gives an intermittent nature to fire spread for constant external conditions. This is primarily due to the reduced convective cooling of the pine needles in comparison with cardboard combs. The flame contact causes point ignitions that give a leaping character to fire spread. This leaping behaviour has not been explored previously and requires attention as it may scale up for large-scale experiments, causing significant acceleration of the fire front. However, large-scale experiments are required to completely understand this phenomenon. In addition to fire movement along the fuel surface, fire behaviour within the fuel bed was measured using thermocouples and pressure probes embedded inside the bed.

Materials and methods

Wind and fire interactions influence instantaneous fire behaviour, impacting spread through the fuel bed. These interactions, along with the fire behaviour, were observed and measured by instrumenting fire spread experiments conducted under varying wind conditions using a well-characterised wind tunnel. This section provides detailed information regarding the experimental set-up and measurement techniques used to conduct and analyse various fire spread experiments performed using vegetative fuel.

Wind tunnel and experimental details

A laboratory-scale wind tunnel was designed and developed for fire research. Three 1.2 m long and 0.8 m^2 cross-section conditioning segments were installed with various honeycomb and perforated sheets to achieve steady and uniform flow in the test section. The test section was designed to hold a test bed to conduct fire spread experiments and contained two doors (top and side) and one window (side) fitted with fire-rated glass for observation and video acquisition. The doors and window provided easy access to the test bed from all directions while maintaining a leakproof test section. A schematic of the wind tunnel test section is presented in Fig. 1, along with the test bed and cameras used during the experiments.

Longleaf pine needles (*Pinus palustris*, PP) and pitch pine needles (*Pinus rigida*, PR) were used for this study with an average fuel moisture content of 6.7 ± 1.15 and $10.14 \pm 0.64\%$ on a dry basis, respectively. Fuel moisture content was measured for each experiment by placing two 15 g samples from the test bed in an oven for 24 h at 60°C (Schemel *et al.* 2008). These pine needles were randomly dispersed across a horizontal test bed shown as a schematic in Fig. 2. The test bed consisted of an unheated plate 465 mm long and 3 mm thick for aerodynamic boundary layer development. A sand layer was used as the insulating base for the pine needles to imitate the natural environment. Horizontal side extensions of dimensions 100×2115 mm (not shown in the figure) were added to both sides of the test bed. These extensions were flush with the sand surface and were placed to prevent any flow circulation between the top and bottom of the test bed. Pine needles were ignited using a fuel wick of size 15 mm by 600 mm soaked in liquid methanol. A thin nickel-chromium wire (0.33 mm in diameter) was heated using a high-voltage signal and placed across
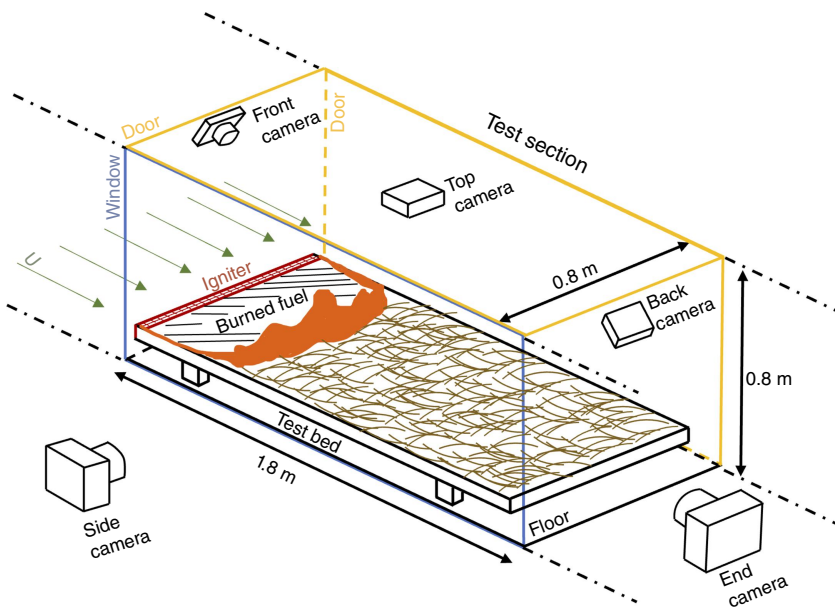
Fig. 1. Schematic of the test section of the lab-scale wind tunnel used for fire spread experiments along with the test bed and cameras used for video acquisition.
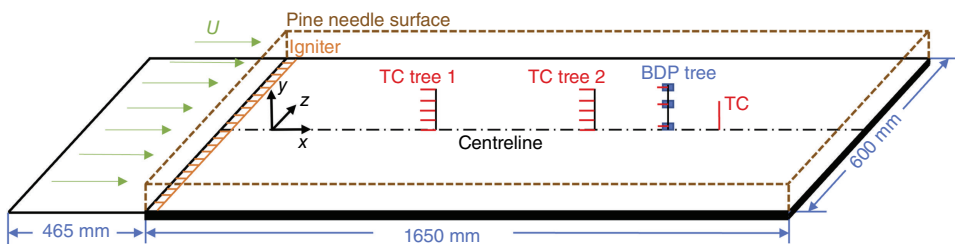

Fig. 2. Test bed schematic showing instrumentation used for fire behaviour measurements. TC, thermocouple; BDP, bi-directional probe.

the width of the wick to ignite the methanol. Various temperature and velocity probes were placed along the centreline of the test bed to measure fire behaviour.

Fire spread experiments were conducted under five different wind conditions, namely 0, 0.23, 0.42, 0.75 and $1.38 \, \mathrm{m \, s^{-1}}$. Low to medium wind velocity was used for these experiments. This study focused on understanding fire spread during the low-intensity surface fires commonly observed during small-scale wildland fires and prescribed burns. The highest velocity was also restricted by the possible displacement of burning pine needles owing to weight loss during combustion. Each experiment was conducted four times for repeatability, and a 95% confidence interval was used to measure the error in the mean values.

The available wind tunnel height, reduced to 0.65 m by the test bed, was a limiting factor for the maximum fuel loading. PP was distributed across the test bed with a fuel loading of $0.5 \, \mathrm{kg \, m^{-2}}$ (495 g) as a higher value led to flame contact with the ceiling. In comparison, PR was distributed with a fuel loading of $0.8 \, \mathrm{kg \, m^{-2}}$ (792 g) for two reasons. The maximum values of total heat flux incident at the fuel surface were compared between PP and PR for the same fuel loading of $0.5 \, \mathrm{kg \, m^{-2}}$ and wind velocity of $0.23 \, \mathrm{m \, s^{-1}}$. The average value of total heat flux measured for PP was $40 \, \mathrm{kW \, m^{-2}}$, whereas the total heat flux generated by PR

for a fuel loading of $0.5 \, \mathrm{kg \, m^{-2}}$ was $8.21 \, \mathrm{kW \, m^{-2}}$, hence a reduction of 79.5%, which was significantly low. However, on increasing the fuel loading to $0.8 \, \mathrm{kg \, m^{-2}}$, the total heat flux generated by the flame was $26.9 \, \mathrm{kW \, m^{-2}}$, which was still lower than PP, but the reduction was 32.75%.

Furthermore, one of the objectives of this work was to evaluate flame movement within the fuel bed, which was achieved using thermocouple trees consisting of five thermocouples. Four thermocouples were placed within the pine needle bed, while the fifth was kept outside the bed. This could not be achieved for PR with a fuel loading of $0.5 \, \mathrm{kg \, m^{-2}}$ as the fuel bed height was less than 3 cm. Therefore, the fuel loading for PR was increased to $0.8 \, \mathrm{kg \, m^{-2}}$, which increased the fuel bed height to 5 cm.

Instrumentation details

Fire behaviour was measured using various instruments strategically placed in and around the test bed. The schematic in Fig. 2 shows all the instruments placed inside the test bed, while Fig. 1 shows the cameras used for fire behaviour observation. Five cameras were used around the test bed, with the side and end camera capturing videos at 120 frames per second with the rest captured at 60 frames per second. The videos acquired were analysed using

techniques described in the following sub-section. Gas temperature was measured using thermocouples placed along the centreline of the test bed at four x-locations. Two thermocouple trees were placed at $x = 54$ cm and $x = 104$ cm. Each tree consisted of five equally spaced K-type thermocouples with the spatial details presented in Table 1. The K-type thermocouples used here were $150\,\mu$m in diameter with Inconel® 600 sheathing. Temperature measurements were conducted at a sampling frequency of 75 Hz.

A Bi-Directional Probe (BDP) tree consisting of three BDPs was used to measure the pressure gradient established by the flame and converted to instantaneous gas velocity. A K-type thermocouple was attached to each BDP for density correction and flame location measurement. Each BDP was 10 mm in diameter and placed along the centreline of the test bed with additional location details presented in Table 1. A differential pressure transducer (Sensirion SDP810-125 Pa) digitised the probe measurements at a nominal frequency of 150 Hz, which was resampled to 75 Hz for density correction and velocity conversion. Accurate velocity conversion required the measurement of an amplification factor or K-factor for the BDP, calculated using Eqn 1 where V_{actual} corresponds to the velocity measured using a Pitot tube. ΔP_{BDP} represents the differential pressure measured using BDP and ρ_∞ is the ambient air density.

$$K_{\text{BDP}} = \frac{V_{\text{actual}}}{(2\Delta P_{\text{BDP}}/\rho_\infty)^{0.5}} \qquad (1)$$

The K-factor was evaluated using 46 different pressure conditions established by varying the Variable Frequency Drive (VFD) frequency, which changed the fan revolutions per minute (RPM). Fig. 3*a* shows the K-factor variation with the measured pressure gradient for the 46 pressure points.

It can be seen that the K-factor varies significantly for low-pressure values (up to 0.5 Pa) and stagnates at ~1.8 above it. This variation in values prevented approximating a single K-factor for the BDP. Therefore, a piecewise function was established for calculating the K-factor for measured differential pressure. The piecewise function presented in Eqn 2 consisted of a fourth-order polynomial up to a pressure ΔP of 0.25 Pa and a power-law function for pressure values greater than or equal to 0.25 Pa. Velocity values were calculated using this function and are compared with the actual velocity measured using a Pitot tube in Fig. 3*b* for different VFD frequencies. Fig. 3*b* also shows the error percentage ($= (V_{\text{BDP}} - V_{\text{actual}}) \times 100/V_{\text{actual}}$) for each velocity value along with the raw BDP velocity calculated without the K-factor. A maximum absolute error of 11.35% was observed, which was acceptable for the range of pressure measurements.

$$
K_{\text{BDP}}(\Delta P) =
\begin{cases}
-9530.7(\Delta P)^4 + 5089.9(\Delta P)^3 & \Delta P < 0.25 \\
\quad - 917.87(\Delta P)^2 + 64.28(\Delta P) \\
\quad + 0.61, \\
0.006935(\Delta P)^{-3.238} + 1.817, & \Delta P \geq 0.25
\end{cases}
\qquad (2)
$$

The BDP is an intrusive measurement device and was expected to influence flame behaviour. The intrusiveness of the BDP was limited by using a 10 mm diameter probe. To maintain a continuous flame, pine needles were carefully placed between the three BDPs. This ensured a consistent supply of fuel for the spreading flame. The diameter of the probe can be selected as its characteristic length scale, like a sphere. Using this characteristic length, the blockage ratio was 0.012%, which assured

Table 1. Details of thermocouple and bi-directional probe located inside the test bed measured from the igniter leading edge (see Fig. 2).

| Thermocouple tree 1		Thermocouple tree 2		Bi-directional probe tree	
Pinus palustris (fuel bed height = 70 mm)					
$x = 540$ mm	$y = 0$ mm	$x = 1040$ mm	$y = 0$ mm	$x = 1250$ mm	$y = 0$ mm
$x = 540$ mm	$y = 23.3$ mm	$x = 1040$ mm	$y = 23.3$ mm	$x = 1250$ mm	$y = 70.0$ mm
$x = 540$ mm	$y = 46.6$ mm	$x = 1040$ mm	$y = 46.6$ mm		
$x = 540$ mm	$y = 70.0$ mm	$x = 1040$ mm	$y = 70.0$ mm		
$x = 540$ mm	$y = 93.2$ mm	$x = 1040$ mm	$y = 93.2$ mm	$x = 1250$ mm	$y = 93.2$ mm
Pinus rigida (fuel bed height = 50 mm)					
$x = 540$ mm	$y = 0$ mm	$x = 1040$ mm	$y = 0$ mm	$x = 1250$ mm	$y = 0$ mm
$x = 540$ mm	$y = 16.7$ mm	$x = 1040$ mm	$y = 16.7$ mm	$x = 1250$ mm	$y = 50.0$ mm
$x = 540$ mm	$y = 33.4$ mm	$x = 1040$ mm	$y = 33.4$ mm		
$x = 540$ mm	$y = 50.0$ mm	$x = 1040$ mm	$y = 50.0$ mm		
$x = 540$ mm	$y = 66.8$ mm	$x = 1040$ mm	$y = 66.8$ mm	$x = 1250$ mm	$y = 66.8$ mm

D
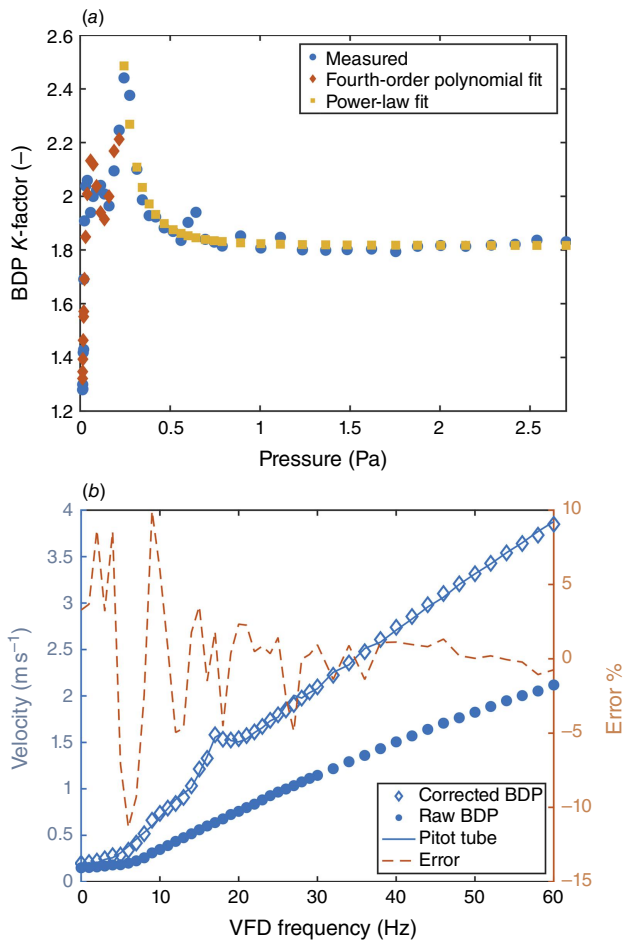
Fig. 3. (*a*) Comparison between the measured and estimated *K*-factor. (*b*) Velocity measured using Pitot tube and bi-directional probe (BDP) against Variable Frequency Drive (VFD) frequency. Raw and corrected values are presented for the BDP along with the associated error for corrected values.

no significant acceleration of wind due to a reduction in the area from the BDP acting as an obstruction.

Video analysis

Front and back view cameras were used to evaluate the average rate of spread (ROS), which was used to validate the flame threshold temperature. These views were used because they observed the complete test bed. Average ROS was calculated by measuring the time required for the flame to move from ignition to the test bed end. A phenomenological understanding of intermittent fire spread was developed by conducting image analysis of side-view videos acquired at 120 frames per second. To quantify this behaviour, a more comprehensive approach is required, which was not in the scope of the current paper. Starting from 400 mm, each video frame was extracted to measure fireline temporal variation. Each frame was binarised to get the furthest fire location along the top surface of the fuel bed.

This analysis was restricted to the middle of the test bed to avoid any parallax error.

Results and discussion

This section presents qualitative and quantitative results from fire spread experiments conducted across PP and PR test beds. It starts with a discussion about the average ROS and then moves on to illustrate the impact of dynamic fire behaviour on flame propagation using various videos. Temperature and velocity measurements were acquired to build on the understanding obtained from video analysis.

Flame spread

Average flame spread

Understanding flame spread behaviour under varying external conditions assists in building and validating reliable fire prediction models. A significant portion of the fire literature provides a dataset on the variation of average ROS with wind, vegetation and topology. The present work adds to that dataset while providing a fundamental understanding of dynamic fire behaviour and intermittent flame spread. The average ROS (in $cm\,s^{-1}$) was evaluated using four thermocouples at $x = 54, 104, 125$ and $140\,cm$. These thermocouples were placed along the fuel surface at $y = 7\,cm$ and $y = 5\,cm$ for PP and PR, respectively. Flame presence was approximated by taking a threshold temperature of $573.15\,K$ (300°C) following previous work by Mueller *et al.* (2018). Fig. 4*a* presents an example of average ROS calculation where the four data points represent the thermocouple streamwise location and the corresponding time instant when the flame reaches the thermocouple. Average ROS was equal to the slope of a linear fit between the four data points, which always showed a regression greater than 0.95. The value next to each data point corresponds to the first temperature value (in K) that exceeds the threshold of $573.15\,K$.

The above technique was validated in Fig. 4*b* by comparison against the average ROS measured using videos acquired by cameras placed around the test bed. Front and back view videos were separately analysed, and ROS was evaluated for the entire bed. The average ROS from the videos was then taken as the mean of the ROS from both views. Each experiment was repeated four times. The average ROS (video and temperature) shown in Fig. 4*b* presents the mean of all the experiments with the error bar calculated using a 95% confidence interval. Average ROS measured using thermocouples is mostly underpredicted, with a maximum percentage difference of 20%, which lies within the error bars. This underprediction was reasonable as thermocouples start from $x = 54\,cm$ and neglect the initial acceleration on ignition that was captured by the videos. It was concluded from this analysis that a threshold temperature of $573.15\,K$ or 300°C was applicable for the current set of experiments.
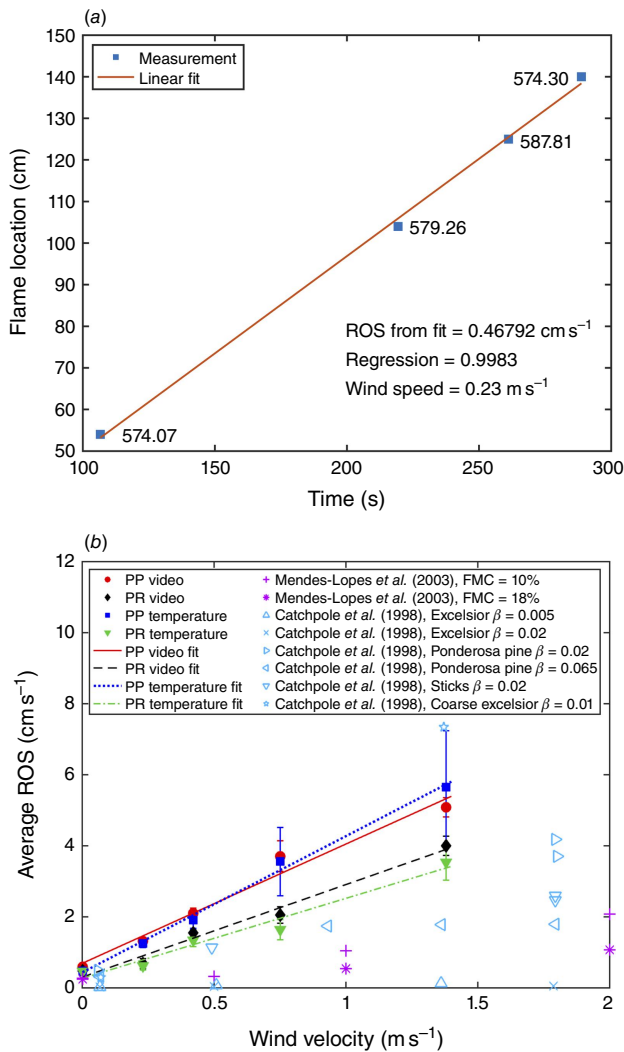
Fig. 4. (*a*) Example of average ROS evaluation using threshold temperature for four thermocouples at the fuel bed surface. (*b*) Variation of average ROS with wind and comparison between different ROS measurement techniques.

Temporal variation of the fireline

Temporal variation of the fireline was measured along the test bed using the side-view videos acquired at a frequency of 120 Hz and is presented in Fig. 5. An algorithm was developed to acquire the fireline location from these videos by converting individual frames to binary images. The fuel bed surface was taken as the reference, and fireline location was measured along this reference line for each experiment. This reference line varied between PR and PP as the fuels had different fuel bed heights, 5 and 7 cm, respectively. The analysis was initiated when the flame approached the 40 cm mark to avoid parallax errors and allow flame development.

The analysis presented in Fig. 5 was restricted to 16 s, totaling 1920 frames, and required significant computing capacity. The slope of the curve in Fig. 5 represents the

flame spread rate, and an increasing trend was observed with wind velocity for both fuels. This behaviour was similar to that measured from the thermocouple and other camera views in the previous sub-section. The more critical understanding gained from this figure was the presence of fluctuations. These fluctuations represent the point ignitions ahead of the fireline or the near-bed flame pulsations occurring when the wind cuts across the flame front. The magnitude of the fluctuations increased with increasing wind because of the more substantial influence of wind and fire interactions. These interactions are known to be one of the controlling parameters for generating near-bed pulsations and point ignitions and are further explored in the next section.

An interesting flame spread behaviour was observed in Fig. 5, where the continuously rising curve also had flat regions or plateaus. These plateaus occur because of flame residence and indicate intermittent flame movement along the fuel surface. This intermittent flame movement was observed as leaps and was analysed using other camera views. The flame residence time was more significant for no- to low-wind conditions and decreased for higher winds. A lower residence time allowed for less fuel involvement under the top surface. For higher wind conditions, the fuel underneath the top surface burned after the flame moved to a new streamwise location, and a trailing fire was observed.

Dynamic fire behaviour

This section explores the origin of intermittent flame spread behaviour discussed in the previous section. The inherently dynamic nature of free-burning fires was closely observed from various camera angles and other instrumentation. Viegas (2004*a*) demonstrated the absence of a steady-state burning regime even under nominally uniform and permanent boundary conditions. Flame spread was shown to be an ever-evolving process and can often lead to eruptive fires, as shown by Viegas and Simeoni (2011). Therefore, an understanding of intermittent flame spread behaviour and its origin can assist in the accurate prediction of extreme fire events like eruptive fires (Viegas 2004*b*) and vorticity-driven lateral spread (VLS) (Sharples *et al.* 2012).

Near-bed flame pulsations and point ignitions

Dynamic fire behaviour in the form of flame pulsations was qualitatively examined from the side and back view cameras (refer to Fig. 2). Both camera views were synchronised against the time to ignition and the time series in Fig. 6 was generated to understand the dynamic fire phenomenon. In Fig. 6, each back view frame was placed above the corresponding front view to observe the flame from different angles. Finney *et al.* (2015) observed flame bursts in stationary and spreading flames. These flame bursts contributed to the intermittent rise in temperature of the unburnt fuel ahead of the fireline. Similar puffing behaviour was observed in the current experimental study, focusing on
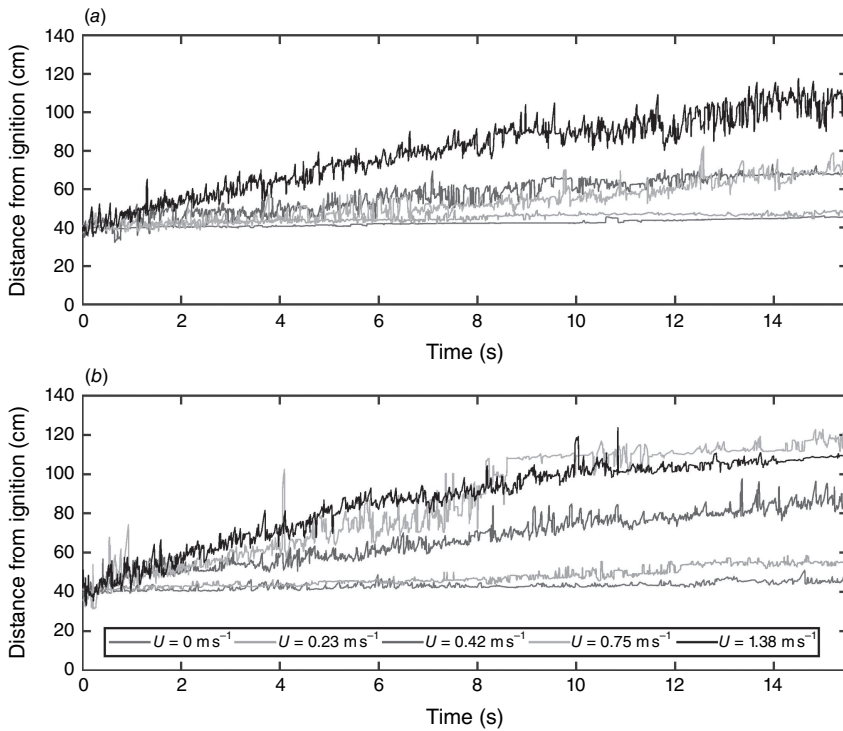
Fig. 5. Temporal variation of the fireline location for (a) *Pinus rigida*, and (b) *Pinus palustris*.
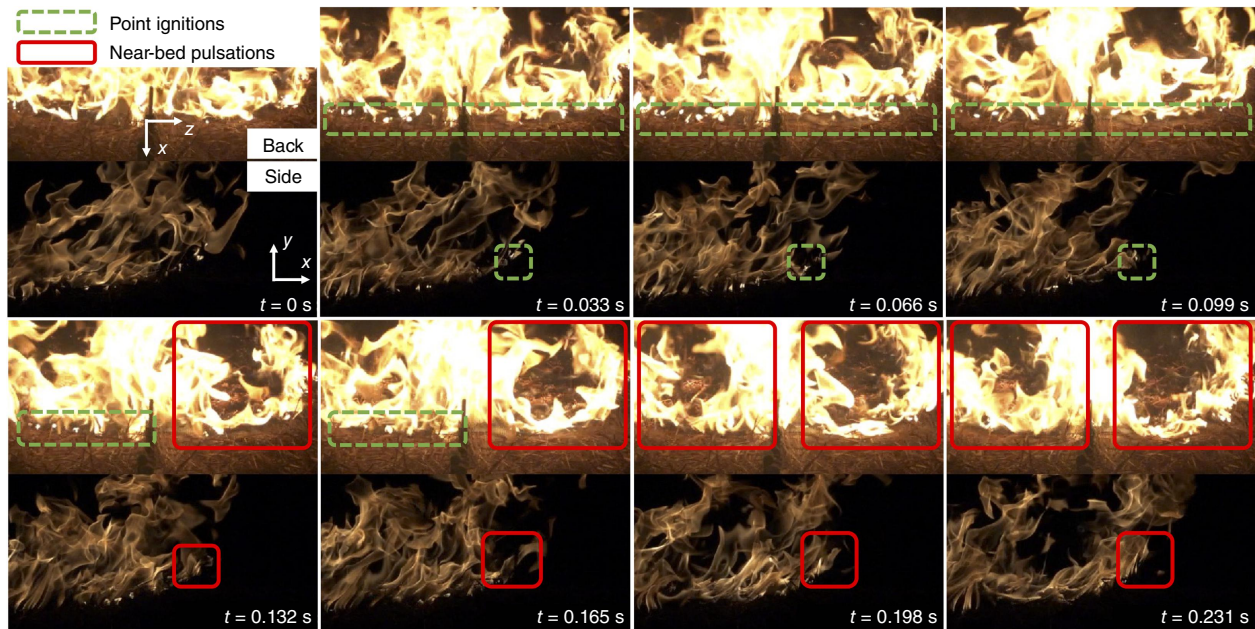

Fig. 6. Back view and side view showing time series of near-bed flame pulsations and point ignitions ahead of fire front for *Pinus rigida* at $U = 0.42 \text{ m s}^{-1}$.

near-bed pulsations and their interaction with fuel and subsequent ignition and flame spread.

The flame front restricts wind movement by acting as a barrier between the unburned and burned fuel regions. The first frame, $t = 0$ s in Fig. 6, shows this flow restriction and

the end of a cyclic process that leads to intermittent flame movement. After the cycle ends, the second frame at $t = 0.033$ s shows multiple point ignitions ahead of the fireline due to radiative preheating and flame contact. These point ignitions represent individual pine needles burning at
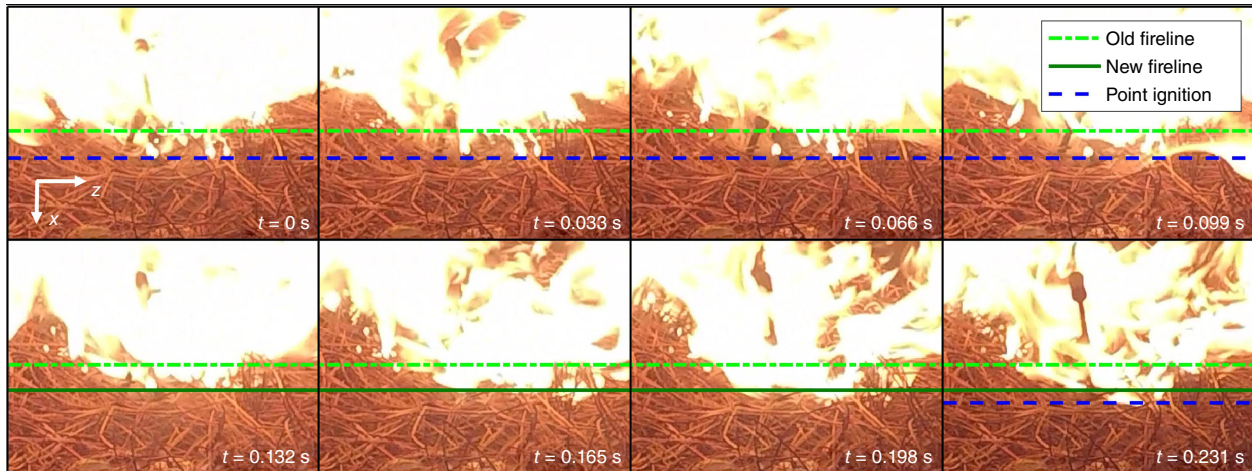
Fig. 7. Point ignitions and corresponding fireline movement in *Pinus palustris* at $U = 0.42 \, \text{m s}^{-1}$ seen from back view.

distinct locations across the width of the test bed. For sustenance, these small free-burning fires require feedback either from the flame front or adjacent point ignitions. The latter was observed to be limited and weak in the cases studied here, while the former was dominant. Heat feedback from the flame front occurred in the form of radiation and convection, with radiation initiating and supporting pyrolysis and flame contact causing point ignitions. Fluctuating flame contact occurred when wind broke through the flame front and pushed it towards the unburned fuel. This process is seen in frames 5 ($t = 0.132 \, \text{s}$) through 8 ($t = 0.231 \, \text{s}$) in Fig. 6, with the wind cutting across from the right and then from the left, generating two troughs and one crest along the centreline. Similar crest and trough structures were observed in previous studies (Beer 1991; Finney *et al.* 2015; Gustenyov *et al.* 2018).

Intermittent flame spread occurred when point ignitions merged with the fireline. This fireline movement was observed in the back view and is presented in Fig. 7 as a time series taken at 1250 mm, which allowed sufficient flame development. Point ignitions occurred on flame contact and required heat feedback for sustenance. The buoyant plume generated a low-pressure zone in the vicinity of the flame and unburnt fuel bringing in cold air from the unburned region in the form of 'fire wind' or fire-induced reverse flow (Smith *et al.* 1975; Hilton *et al.* 2018). This inhibited the existence of point ignitions by negating the heat feedback from the flame. The blue dotted line represents point ignitions in Fig. 7, and the old fireline is shown using a green line. Under favourable heating conditions, the point ignitions grew in number and eventually merged with the old fireline to generate the new fireline. This new fireline was not adjacent to the old fireline but a bit further, suggesting flame movement occurred in the form of leaps. This behaviour was further observed with new point ignitions ahead of the fireline in the last frame at $t = 0.231 \, \text{s}$.

Local flow variation

A qualitative understanding of point ignitions and intermittent flame spread was established in the previous section. Fire-induced flow was also discussed and presented as one of the parameters affecting point ignitions, and required more understanding. For this purpose, BDPs were placed along the test bed centreline to measure the local differential pressure. This pressure was converted to instantaneous velocity using the corresponding density and *K*-factor.

Velocity measured at the fuel surface was compared for different wind conditions for both fuels in Figs 8 and 9. Positive values correspond to gas flow along the flame spread direction. A thin K-type thermocouple attached to the BDP was used to evaluate flame presence by taking a threshold of 573.15 K. Under zero wind conditions, when the flame approached the BDP, the average zero flow decreased to slightly negative values, representing fire-induced reverse flow. The negative flow was sustained and increased for approximately up to half of the flame and then became positive. This behaviour can be understood by looking into zero-flow flame geometry (Mendes-Lopes *et al.* 2003). Flame tilt away from the unburned fuel bed generated negative flow when the flame was behind the middle of the BDP. As the flame moved and completely engulfed the BDP, positive flow dominated the inverse flow. After the flame front moved ahead of the BDP, as observed by the thermocouple, the trailing flame was sustained and produced the positive flow, as seen in Figs 8 and 9.

Local flow velocity was also measured for the four cases of wind-aided fires presented in Figs 8 and 9 with no negative flow within the shaded region. This behaviour can be similarly understood from the flame geometry of wind-aided fires. Negative values were observed only for low-wind conditions, but reduced positive values for higher winds showed that the presence of fire-induced reverse flow influenced local flow. As the flame engulfed the BDP, positive
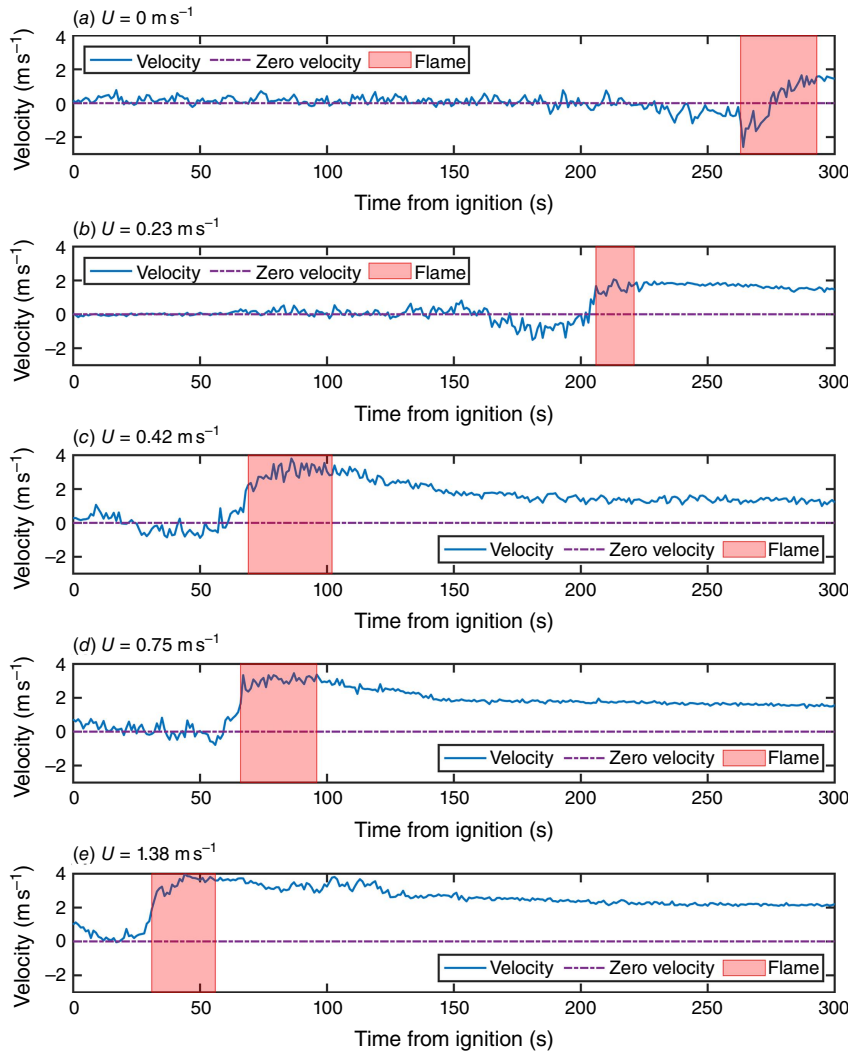
Fig. 8. Instantaneous velocity variation for BDP at the fuel bed surface of *Pinus rigida* under varying wind conditions of (a) $U = 0\,\text{m s}^{-1}$, (b) $U = 0.23\,\text{m s}^{-1}$, (c) $U = 0.42\,\text{m s}^{-1}$, (d) $U = 0.75\,\text{m s}^{-1}$ and (e) $U = 1.38\,\text{m s}^{-1}$.

flow increased, reaching a maximum. This value slowly dropped and reached a constant value dependent on the external wind and trailing fire. For all the wind cases studied in this work, similar flow trends were observed for both the pine needles but at different magnitudes. PP showed a higher maximum velocity as compared with PR. A complete understanding of this behaviour requires a detailed analysis of fire intensity and fuel properties, which was not an objective of this study.

Fire behaviour inside the fuel bed

The analysis up to now considers flame spread and fire behaviour across the fuel bed surface; this last section shifts the focus to fire behaviour within the fuel bed. This was important for completeness of studying the problem and building further insight into flame leaping. Bi-directional probes and thermocouples were embedded inside the fuel bed to measure instantaneous flow and temperature within the bed.

Velocity variation within the fuel bed

Three BDPs placed at one streamwise location in a vertical arrangement captured the local flow within, at and above the fuel surface for both fuels. A thin K-type thermocouple accompanied each BDP for density correction and flame presence evaluation. Before the flame approach, near-zero flow was recorded by the bottom BDP for both fuels under different wind conditions, as shown in Figs 10 and 11. The porous vegetative fuel restricts the flow of wind through the fuel bed. As the flame propagated towards the BDP, fire-induced flow generated a reverse flow leading to a dip in the velocity curve. After the drop, as the flame reached the BDP, the local flow velocity attained the peak value and then slowly decreased to ambient conditions.

Flow blockage by the fuel diminished moving towards the top surface of the fuel bed (*y*-direction), with the middle BDP observing reduced flow while the top BDP observed the ambient wind before flame approach. This behaviour was
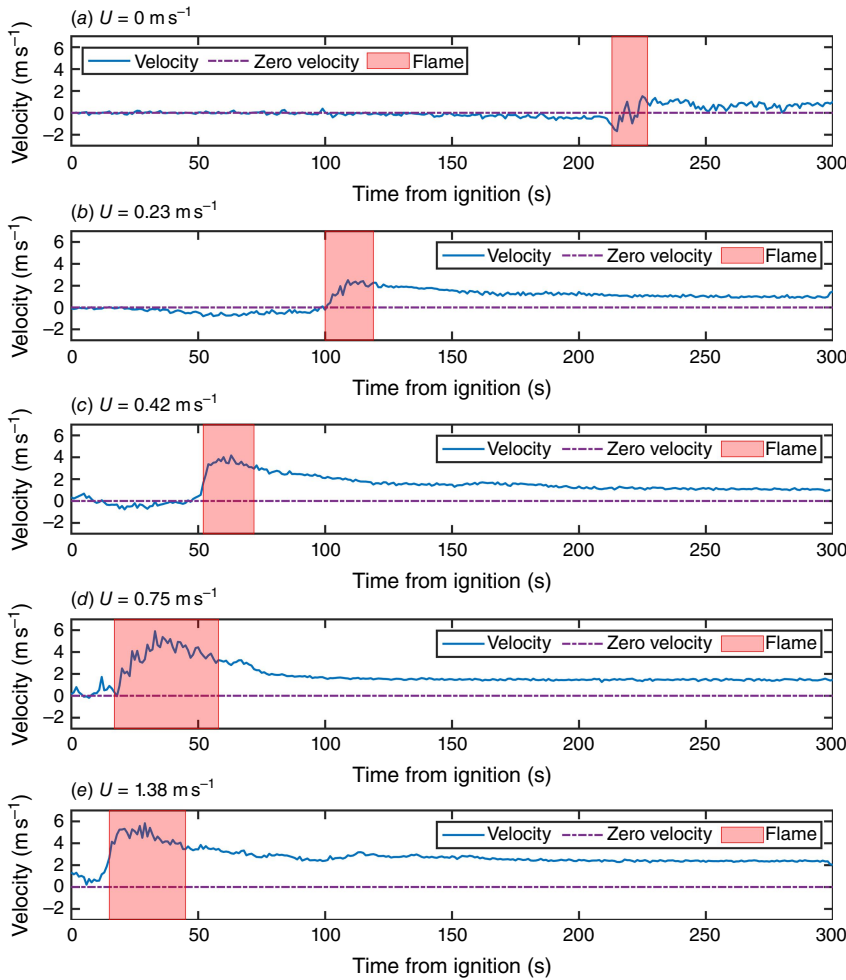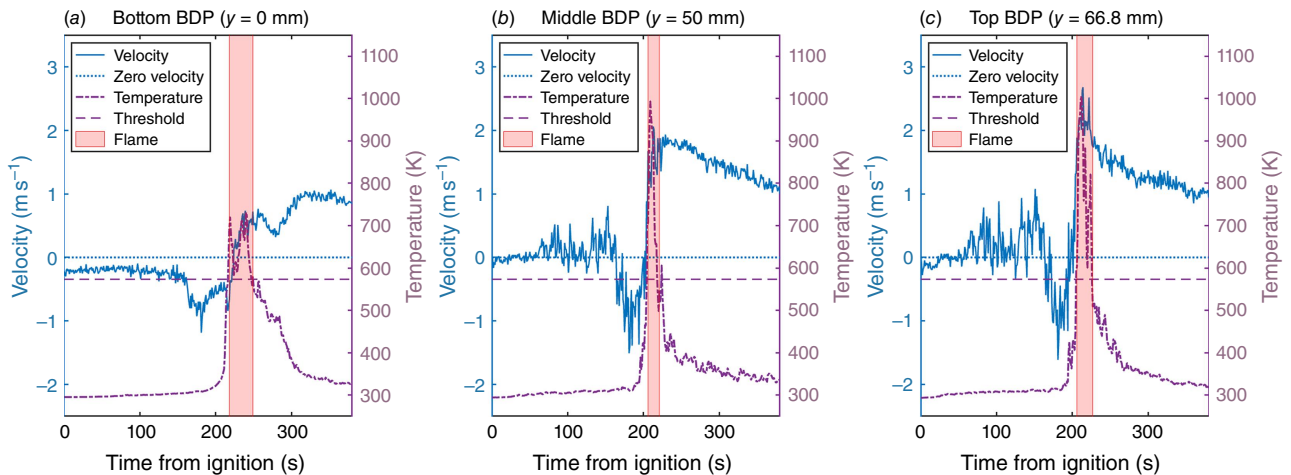
I

Fig. 9. Instantaneous velocity variation for BDP at the fuel bed surface of *Pinus palustris* under varying wind conditions of (*a*) $U = 0\,\mathrm{m\,s^{-1}}$, (*b*) $U = 0.23\,\mathrm{m\,s^{-1}}$, (*c*) $U = 0.42\,\mathrm{m\,s^{-1}}$, (*d*) $U = 0.75\,\mathrm{m\,s^{-1}}$ and (*e*) $U = 1.38\,\mathrm{m\,s^{-1}}$.

Fig. 10. Comparison of velocity and temperature measured by BDP at various vertical locations, (*a*) $y = 0$ mm, (*b*) $y = 50$ mm and (*c*) $y = 66.8$ mm, for $U = 0.23\,\mathrm{m\,s^{-1}}$ for *Pinus rigida*.

similar for both fuels. Reduced flow within the fuel bed suggested a reduction in convective heat transfer and possible dominance of radiation. This decreased the probability of flame contact with the unburned fuel within the fuel bed. Therefore, the point ignitions at the top surface burned independently with little assistance from within the fuel
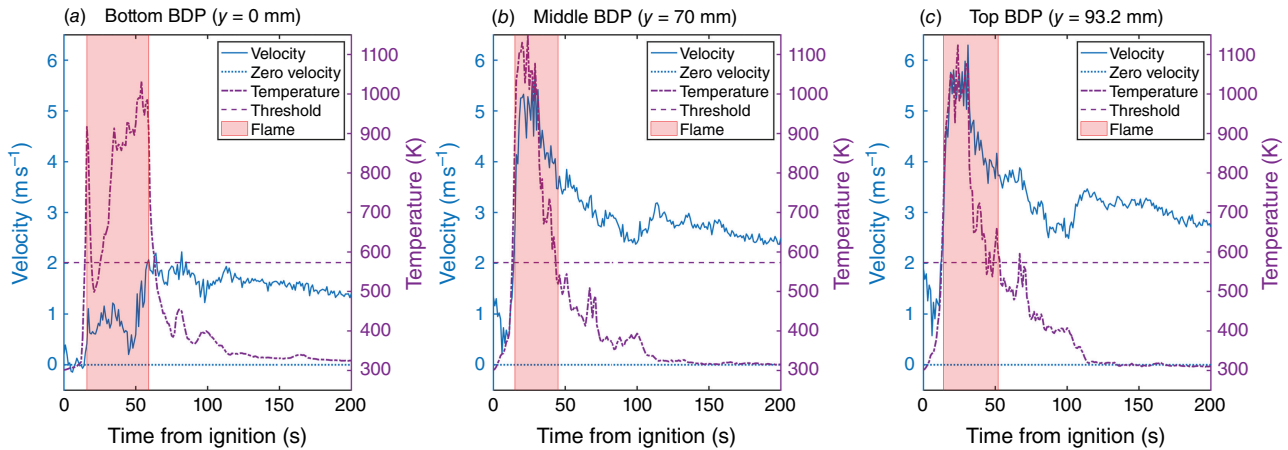
Fig. 11. Comparison of velocity and temperature measured by BDP at various vertical locations, (*a*) *y* = 0 mm, (*b*) *y* = 70 mm and (*c*) *y* = 93.2 mm, for *U* = 1.38 m s^{-1} for *Pinus palustris*.

bed. Additionally, fire propagation inside the bed was expected to be delayed compared with the top surface. This was validated using thermocouple trees placed along the centreline and is discussed in the following sub-section.

Flame spread within the fuel bed

Reduced heat transfer and flame contact probability can cause a possible delay in fire propagation inside the fuel bed. This delay was quantified by placing two thermocouple trees, consisting of five thermocouples each, along the centreline of the fuel bed. The top two thermocouples were placed outside and on the fuel surface, while the other three were embedded inside the fuel. The location details can be found in Table 1.

Corresponding to the previous analysis, flame presence at each thermocouple location was evaluated by taking a threshold of 573.15 K. The top thermocouple was taken as the reference for the time delay as it recorded flame the earliest. The time delay for each thermocouple was calculated by subtracting the reference time from the flaming time at the respective thermocouple location. This led to a zero-time delay for the topmost location and maximum delay for the bottom. The time delay is presented against the vertical (*y*) location in Fig. 12 for Tree 1 in PR and Fig. 13 for Tree 2 in PP.

A fairly flat profile was observed for no wind, suggesting continuous in-depth flame movement. This flatness was lost on introducing the slightest wind, and the top thermocouples experienced flame before the bottom. The curvature of the time delay profile increased with increasing crossflow. This meant the flame skimmed over the top fuel surface while experiencing a delay within the fuel bed for wind-aided fire spread. As the probability of flame contact decreases owing to flow blockage, a more detailed experimental procedure needs to be developed to investigate the mechanism of flame spread inside the bed.
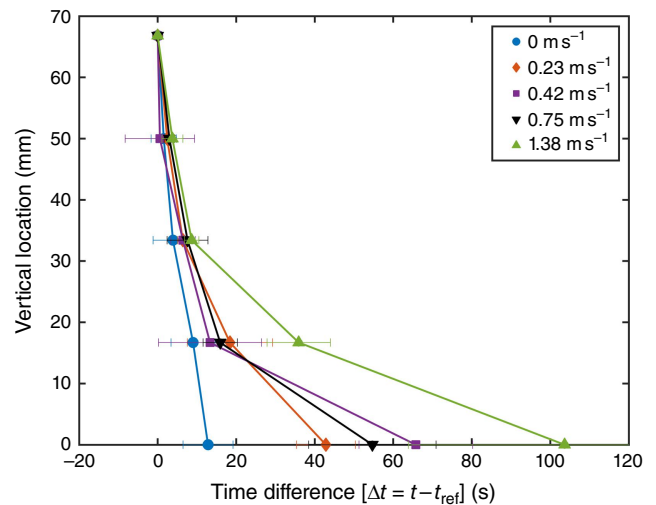

Fig. 12. Flame delay for thermocouples in Tree 1 for *Pinus rigida* under different wind conditions.
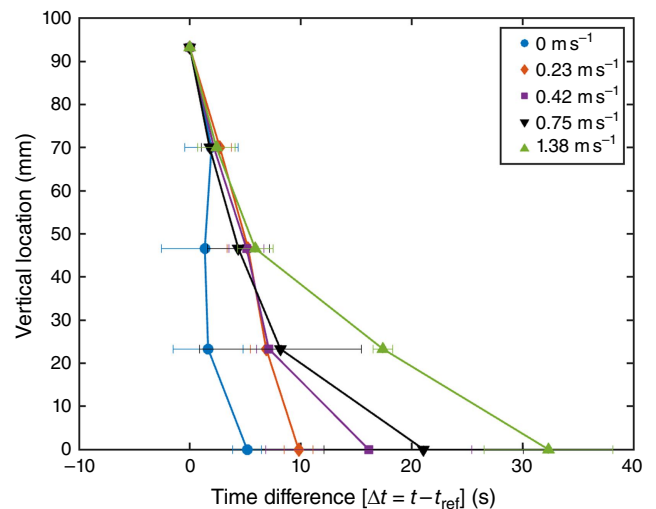

Fig. 13. Flame delay for thermocouples in Tree 2 for *Pinus palustris* under different wind conditions.

Conclusions

Wind effects on fire spread behaviour were explored by conducting experiments in a well-characterised laboratory-scale wind tunnel. A comparison between videos and thermocouple measurements validated the assumption of 573.15 K as a threshold for flame presence. Local fire spread was also evaluated using side view videos, where intermittent fire movement was observed as leaps.

A phenomenological analysis of intermittent fire spread was conducted by closely observing wind and fire interactions from back and side view cameras. Near-bed flame pulsations were observed when the wind cut across the flow obstructing the flame front. These pulsations caused flame contact, leading to point ignitions ahead of the fire front. Favourable heating conditions assisted in the point ignitions merging with the fireline, leading to flame spread in the form of leaps. The fire-induced reverse flow was one of the controlling parameters and varied with the changing external wind. Field-scale experiments are important to understand the influence of point ignitions on fire spread at an increased scale. These experiments have been conducted using a portable field-scale wind tunnel and are currently under analysis.

Local fire behaviour within the fuel bed was also examined using thermocouples and BDPs. Reduced flow within the fuel bed led to radiation dominance and reduced flame contact, therefore fewer point ignitions and delayed flame movement. This flame delay was also observed and quantified using temperature analysis. This delay increased with increasing wind and was higher for PR, the fuel with a lower permeability due to lower porosity. Further improvements in the current experimental protocol are required to quantify the leaping phenomenon and fire–wind interactions.

References

Albini FA (1985) A model for fire spread in wildland fuels by radiation. *Combustion Science and Technology* **42**, 229–258. doi:10.1080/00102208508960381

Albini FA (1986) Wildland fire spread by radiation – a model including fuel cooling by natural convection. *Combustion Science and Technology* **45**, 101–113. doi:10.1080/00102208608923844

Arnell NW, Lowe JA, Challinor AJ, Osborn TJ (2019) Global and regional impacts of climate change at different levels of global temperature increase. *Climatic Change* **155**, 377–391. doi:10.1007/s10584-019-02464-z

Atkinson GT, Drysdale DD, Wu Y (1995) Fire driven flow in an inclined trench. *Fire Safety Journal* **25**, 141–158. doi:10.1016/0379-7112(95)00039-9

Beer T (1991) The interaction of wind and fire. *Boundary-Layer Meteorology* **54**, 287–308. doi:10.1007/BF00183958

Brown A, Davis K (1973) Fire in North American Forests. In 'Forest fire: control and use'. (Ed. K Davis) pp. 15–44. (McGraw Hill Series in Forest Resources)

Catchpole WR, Catchpole EA, Butler BW, Rothermel RC, Morris GA, Latham DJ (1998) Rate of spread of free-burning fires in woody fuels in a wind tunnel. *Combustion Science and Technology* **131**, 1–37. doi:10.1080/00102209808935753

Dupuy JL (1995) Slope and fuel load effects on fire behavior: laboratory experiments in pine needles fuel beds. *International Journal of Wildland Fire* **5**, 153–164. doi:10.1071/WF9950153

Finney MA, Cohen JD, Forthofer JM, McAllister SS, Gollner MJ, Gorham DJ, Saito K, Akafuah NK, Adam BA, English JD (2015) Role of buoyant flame dynamics in wildfire spread. *Proceedings of the National Academy of Sciences* **112**, 9833–9838. doi:10.1073/pnas.1504498112

Gustenyov N, Akafuah NK, Salaimeh A, Finney M, McAllister S, Saito K (2018) Scaling non-reactive cross flow over a heated plate to simulate forest fires. *Combustion and Flame* **197**, 340–354. doi:10.1016/j.combustflame.2018.08.014

Hann WJ, Bunnell DL (2001) Fire and land management planning and implementation across multiple scales. *International Journal of Wildland Fire* **10**, 389–403. doi:10.1071/wf01037

Hilton JE, Sullivan AL, Swedosh W, Sharples J, Thomas C (2018) Incorporating convective feedback in wildfire simulations using pyrogenic potential. *Environmental Modelling & Software* **107**, 12–24. doi:10.1016/j.envsoft.2018.05.009

Kimmerer RW, Lake FK (2001) The role of indigenous burning in land management. *Journal of Forestry* **99**, 36–41. doi:10.1093/jof/99.11.36

Lin Y, Hu L, Zhang X, Chen Y (2021) Experimental study of pool fire behaviors with nearby inclined surface under cross flow. *Process Safety and Environmental Protection* **148**, 93–103. doi:10.1016/j.psep.2020.10.011

Liu N, Lei J, Gao W, Chen H, Xie X (2021) Combustion dynamics of large-scale wildfires. *Proceedings of the Combustion Institute* **38**, 157–198. doi:10.1016/j.proci.2020.11.006

McAllister S, Finney M (2016) Burning rates of wood cribs with implications for wildland fires. *Fire Technology* **52**, 1755–1777. doi:10.1007/s10694-015-0543-5

Mendes-Lopes JMC, Ventura JMP, Amaral JMP (2003) Flame characteristics, temperature-time curves, and rate of spread in fires propagating in a bed of *Pinus pinaster* needles. *International Journal of Wildland Fire* **12**, 67–84. doi:10.1071/WF02063

Mueller EV, Skowronski N, Thomas JC, Clark K, Gallagher MR, Hadden R, Mell W, Simeoni A (2018) Local measurements of wildland fire dynamics in a field-scale experiment. *Combustion and Flame* **194**, 452–463. doi:10.1016/j.combustflame.2018.05.028

Pastor E, Àgueda A, Andrade-Cetto J, Muñoz M, Pérez Y, Planas E (2006) Computing the rate of spread of linear flame fronts by thermal image processing. *Fire Safety Journal* **41**, 569–579. doi:10.1016/j.firesaf.2006.05.009

Perry GLW (1998) Current approaches to modelling the spread of wildland fire: a review. *Progress in Physical Geography: Earth and Environment* **22**, 222–245. doi:10.1177/030913339802200204

Radeloff VC, Helmers DP, Anu Kramer H, Mockrin MH, Alexandre PM, Bar-Massada A, Butsic V, Hawbaker TJ, Martinuzzi S, Syphard AD, Stewart SI (2018) Rapid growth of the US wildland–urban interface raises wildfire risk. *Proceedings of the National Academy of Sciences* **115**, 3314–3319. doi:10.1073/pnas.1718850115

Romero S (2022) The Government Set a Colossal Wildfire. What Are Victims Owed? (21 June 2022) *New York Times*. Available at https://www.nytimes.com/2022/06/21/us/new-mexico-wildfire-forest-service.html [verified 28 June 2022]

Rothermel RC (1972) A mathematical model for predicting fire spread in wildland fuels. Research Paper INT-RP-115. (USDA Intermountain Forest and Range Experiment Station: Ogden, UT) Available at https://www.fs.usda.gov/treesearch/pubs/32533

Schemel CF, Simeoni A, Biteau H, Rivera JD, Torero JL (2008) A calorimetric study of wildland fuels. *Experimental Thermal and Fluid Science* **32**, 1381–1389. doi:10.1016/j.expthermflusci.2007.11.011

Sharples JJ, McRae RHD, Wilkes SR (2012) Wind–terrain effects on the propagation of wildfires in rugged terrain: Fire channelling. *International Journal of Wildland Fire* **21**, 282–296. doi:10.1071/WF10055

Simeoni A (2013) Experimental understanding of wildland fires. In 'Fire Phenomena and the Earth System'. (Ed. C Belcher) pp. 35–52 (John Wiley & Sons: Oxford) doi:10.1002/9781118529539

Simpson CC, Sharples JJ, Evans JP (2014) Resolving vorticity-driven lateral fire spread using the WRF-Fire coupled atmosphere–fire numerical model. *Natural Hazards and Earth System Sciences* **14**, 2359–2371. doi:10.5194/nhess-14-2359-2014

Smith DA (1992) Measurements of flame length and flame angle in an inclined trench. *Fire Safety Journal* **18**, 231–244. doi:10.1016/0379-7112(92)90017-7

Smith RK, Morton BR, Leslie LM (1975) The role of dynamic pressure in generating fire wind. *Journal of Fluid Mechanics* **68**, 1–19. doi:10.1017/S0022112075000651

Sullivan AL (2009*a*) Wildland surface fire spread modelling, 1990–2007. 1: Physical and quasi-physical models. *International Journal of Wildland Fire* **18**, 349–368. doi:10.1071/WF06143

Sullivan AL (2009*b*) Wildland surface fire spread modelling, 1990–2007. 3: Simulation and mathematical analogue models. *International Journal of Wildland Fire* **18**, 387–403. doi:10.1071/WF06144

Sullivan AL (2009*c*) Wildland surface fire spread modelling, 1990–2007. 2: Empirical and quasi-empirical models. *International Journal of Wildland Fire* **18**, 369–386. doi:10.1071/WF06142

Tang W, Finney M, McAllister S, Gollner M (2019) An experimental study of intermittent heating frequencies from wind-driven flames. *Frontiers in Mechanical Engineering* **5**, 34. doi:10.3389/fmech.2019.00034

Trauernicht C, Brook BW, Murphy BP, Williamson GJ, Bowman DMJS (2015) Local and global pyrogeographic evidence that indigenous fire management creates pyrodiversity. *Ecology and Evolution* **5**, 1908–1918. doi:10.1002/ece3.1494

Viegas DX (2004*a*) On the existence of a steady state regime for slope and wind-driven fires. *International Journal of Wildland Fire* **13**, 101–117. doi:10.1071/WF03008

Viegas DX (2004*b*) A mathematical model for forest fires blowup. *Combustion Science and Technology* **177**, 27–51. doi:10.1080/00102200590883624

Viegas DX, Simeoni A (2011) Eruptive behaviour of forest fires. *Fire Technology* **47**, 303–320. doi:10.1007/s10694-010-0193-6

Viegas DXFC, Raposo JRN, Ribeiro CFM, Reis LCD, Abouali A, Viegas CXP (2021) On the non-monotonic behaviour of fire spread. *International Journal of Wildland Fire* **30**, 702–719. doi:10.1071/WF21016

Author affiliation
[A]Department of Fire Protection Engineering, Worcester Polytechnic Institute, Worcester, MA, USA.